Freie Universität Berlin

Fachbereich Chemie

Understanding the oxidation mechanism of formic acid on transition metal electrodes

Bachelor Thesis

vorgelegt von

Jenny Linde

Erstprüfer: Prof. Dr. Martin Wolf

Zweitprüfer: Prof. Dr. Thomas Risse

Juli 2014

Diese Arbeit entstand in der Abteilung Physikalische Chemie von
Prof. Dr. Martin Wolf am Fritz-Haber-Institut Berlin

Berlin, im Juli 2014

Contents

1. Introduction

The history of investigating the electrooxidation mechanism of formic acid dates as far back as 1923, when Müller was the first to recognize that the oxidation proceeds through two different mechanisms on platinum. He also found evidence of an electrocatalytic poison which today is know to be adsorbed carbon monoxide [1]. The interest in this particular reaction at that time was mainly due to it being a simple model for the electrooxidation of small organics like methanol or formaldehyde.

In the past this interest has increased due to the further development of proton exchange membrane fuel cells (PEMFC). These low temperature fuel cells produce electrical energy by converting the chemical energy of the reaction of hydrogen and oxygen. This is done in a cell with a membrane electrode assembly consisting of a solid electrolyte membrane (e.g. Nafion®) with a platinum based catalyst on its sides as electrodes. Air on the cathodic side provides the necessary oxygen while hydrogen is used as fuel. The single cells are combined to fuel cell stacks to achieve the required power. Due to its high cost the main use is in space technology and the military. For reaching the aim of replacing internal combustion engines and conventional power stations PEMFCs have to be further improved [2].

The first improvement was to replace the hydrogen gas with liquid methanol and reforming it to hydrogen inside the cell [3]. Later direct methanol fuel cells (DMFC) were developed where methanol itself is the fuel. The advantage of these cells is the simplified handling and increased miniaturization potential by using a liquid instead of a gas. On the other hand they have a lower electrocatalytic oxidation rate and decreased efficiency due to the usage of low concentrations which are necessary to minimized the performance loss caused by the cross–over of unused methanol through the Nafion® membrane [4]. Despite their limitations both fuel cells are considered the dominant choices for replacing batteries in portable electronic devices [3].

Lately another fuel is considered in the field of portable applications – formic acid. Formic acid has the advantage of being a stable, non–toxic liquid at room temperature with a small cross–over flux through Nafion®. This allows higher concentrated solutions and a thinner membrane compared to methanol. In addition

direct formic acid fuel cells have a higher open circuit potential than both PEMFCs and DMFCs [5]. For further improvement of these cells a better understanding of the electrooxidation of formic acid with different electrodes is important.

In 1967 Breiter et al. were the first to observe adsorbed intermediates other than CO during the oxidation of methanol, formic acid and formaldehyde on platinum [6] and Capon et al. proposed different adsorbates for the dual pathway oxidation in 1973 [7]. The dual pathway mechanism consists of the dehydration of formic acid to adsorbed CO and subsequent oxidation to CO_2 as the indirect pathway and the direct pathway via an unknown adsorbed species. Later other electrode materials were considered due to the CO poisoning effect on platinum and 1992 Hamelin et al. proposed the existence of only the direct pathway for the oxidation of formic acid on gold [8].

Many possible molecules were discussed as the adsorbed species in the direct pathway and in 2002 Miki et al. were the first to confirm adsorbed formate as the active intermediate on platinum [9]. Beltramo et al. found in 2005 that it is also the active intermediate on gold. The existence of adsorbed formate as active intermediate on both platinum and gold is now widely acknowledged but the possibility of a different adsorbate geometry like COOH is not ruled out.

The mechanism of the oxidation of adsorbed formate to CO_2 on the other hand is still unsolved. While Beltramo et al. [10] proposed a mechanism via a single adsorbed formate Cuesta et al. [11] proposed a chemical bimolecular reaction between two adsorbed formates on gold. Most recently Gao et al. calculated possible mechanisms on both gold and platinum and addressed the question if the mechanism of the direct pathway is the same on both metals [12].

Using the surface–sensitive spectroscopy method sum frequency generation (SFG) we will probe the adsorbed species on the surface during the electrooxidation of formic acid on gold. SFG has the main advantage that only adsorbed species are probed and even small coverages can be detected. Probing the surface at different frequencies we hope to conclude the argument about the two proposed adsorbate geometries for the direct pathway – COOH and HCOO – and solve the question about the existence of adsorbed HCOOH.

2. Theoretical Concepts

2.1. Sum frequency generation

Sum frequency generation (SFG) is a surface sensitive vibrational spectroscopy method and therefore quite useful for detection and identification of molecules during chemical reactions on surfaces. Another advantage compared to other vibrational spectroscopy methods like IR-Reflection Adsorption Spectroscopy (IRAS) is the up–conversion of the IR with a visible pulse because the detected SFG light will also be in the visible range. This makes it easier to detect due to the higher detection efficiency of CCD–cameras for visible light [13].

For understanding the SFG process a general understanding of linear and nonlinear optics is necessary. The following overview is based on A. Lambert's review paper [14].

Non-coherent light induces a dipole moment in every molecule of the media dependent on the light's electric field and the polarizability α of the molecular electrons which adds to the existing dipole of the material μ_0.

$$\mu = \mu_0 + \alpha E \tag{2.1}$$

On the macroscopic scale of condensed media these dipole moments of the molecules sum up to the bulk polarization P, defined as the dipole moment per volume unit.

$$P = \epsilon_0 \chi \cdot E \tag{2.2}$$

χ describes the macroscopic average of α called linear optical susceptibility of the media and ϵ_0 the vacuum permittivity. The media emits light at the same frequency as the incident light. The stronger the applied electric field the more the non-linearity increases. With pulsed lasers the electric field becomes so strong the linear approximation of the polarization is no longer correct and the higher order terms of the polarization have to be taken into account. This can be described using the

Taylor series.

$$P = P^{(1)} + P^{(2)} + P^{(3)}... \tag{2.3}$$
$$= \epsilon_0 \chi^{(1)} E^{(1)}(r,t) + \epsilon_0 \chi^{(2)} E^{(2)}(r,t) + \epsilon_0 \chi^{(3)} E^{(3)}(r,t)... \tag{2.4}$$

$\chi^{(1)}$ is the linear susceptibility and $\chi^{(i)}$ are the susceptibilities of the i-order.

Assuming two incident laser beams with the electric fields $E_1 \cos(\omega_1 t)$ and $E_2 \cos(\omega_2 t)$ overlap in time and space at the surface, they induce a second order polarization $P^{(2)}$ in the media.

$$P^{(2)} = \epsilon_0 \chi^{(2)} \cdot \Big(E_1 \cos(\omega_1 t) + E_2 \cos(\omega_2 t)\Big)^2 \tag{2.5}$$

Rewriting equation 2.5 gives

$$\begin{aligned} P^{(2)} = \frac{1}{2}\epsilon_0 \chi^{(2)} \Big[E_1^2(1 + \cos(2\omega_1)t) + E_2^2(1 + \cos(2\omega_2)t)\Big] \\ + \epsilon_0 \chi^{(2)} \Big[E_1 E_2(\cos(\omega_1 + \omega_2)t + \cos(\omega_1 - \omega_2)t\Big] \end{aligned} \tag{2.6}$$

This shows the polarized media can emit light at the frequencies $2\omega_1$, $2\omega_2$, $\omega_1 + \omega_2$ and $\omega_1 - \omega_2$ because of its nonlinear response. This emitted light corresponds to nonlinear processes of the second order: second harmonic generation ($2\omega_1$ and $2\omega_2$), sum frequency generation ($\omega_1 + \omega_2$) and difference frequency generation ($\omega_1 - \omega_2$). Concentrating on the relevant process for this thesis (SFG) ω_1 becomes ω_{vis} corresponding to the visible beam and ω_2 becomes ω_{IR} corresponding to the IR beam. The induced polarization of the SFG process becomes:

$$P^{(2)}_{SFG} = \epsilon_0 \chi^{(2)} E_{vis} E_{IR} \tag{2.7}$$

The incoming IR beam excites a molecular vibration at the interface and the visible beam overlapping in time and space excites the SFG process. Considering energy conservation the SFG process can be described as follows.

$$\omega_{SFG} = \omega_{vis} + \omega_{IR} \tag{2.8}$$

The momentum conservation of the process parallel to the surface gives

$$\omega_{SFG} \cdot \sin\beta_{SFG} = \omega_{vis} \cdot \sin\beta_{vis} + \omega_{IR} \sin\beta_{IR} \tag{2.9}$$

with β_{SFG}, β_{vis} and β_{IR} being the beam angles in respect to the surface normal [14]. This shows the angle of the emitted SFG light depends on the angles of the incident beams.

As it is shown in equation 2.7 the induced polarization is proportional to the electric fields of the incoming laser beams. Therefore the intensity of the SFG can be expressed as follows.

$$I_{SFG} \propto \left|P^{(2)}_{SFG}\right|^2 \propto \left|\chi^{(2)}_{eff}\right|^2 I_{vis} I_{IR} \tag{2.10}$$

$\chi^{(2)}_{eff}$ contains all information about the system like polarization or geometrical dependent factors of the interaction of the applied electric fields with adsorbed molecules. $\chi^{(2)}_{eff}$ is a third rank tensor and has 27 components. As the surface of the present study has a macroscopic $C_{\infty v}$ symmetry only seven components are non–zero and just four are independent. In a laboratory frame with (x, y) being the surface plane and z the surface normal the relevant components are $\chi^{(2)}_{zzz}$, $\chi^{(2)}_{zxx} = \chi^{(2)}_{zyy}$, $\chi^{(2)}_{xzx} = \chi^{(2)}_{yzy}$, $\chi^{(2)}_{xxz} = \chi^{(2)}_{yyz}$.

There are four possible polarization combinations that generate SFG on an isotropic surface, but on gold only *ppp* and *ssp* generate a substantial signal.

$\chi^{(2)}_{eff,ssp}$ and $\chi^{(2)}_{eff,ppp}$ can be related to the experimentally controllable parameters including the Fresnel coefficients $L_{ij}(\omega)$ [15].

$$\begin{aligned}
\chi^{(2)}_{eff,ssp} &= L_{yy}(\omega_{SFG}) L_{yy}(\omega_{vis}) L_{zz}(\omega_{IR}) \sin\beta_{IR} \chi^{(2)}_{yyz} \\
\chi^{(2)}_{eff,ppp} &= -\, L_{xx}(\omega_{SFG}) L_{xx}(\omega_{vis}) L_{zz}(\omega_{IR}) \cos\beta_{SFG} \cos\beta_{vis} \sin\beta_{IR} \chi^{(2)}_{xxz} \\
&\quad -\, L_{xx}(\omega_{SFG}) L_{zz}(\omega_{vis}) L_{xx}(\omega_{IR}) \cos\beta_{SFG} \sin\beta_{vis} \cos\beta_{IR} \chi^{(2)}_{xzx} \\
&\quad +\, L_{zz}(\omega_{SFG}) L_{xx}(\omega_{vis}) L_{xx}(\omega_{IR}) \sin\beta_{SFG} \cos\beta_{vis} \cos\beta_{IR} \chi^{(2)}_{zxx} \\
&\quad +\, L_{zz}(\omega_{SFG}) L_{zz}(\omega_{vis}) L_{zz}(\omega_{IR}) \sin\beta_{SFG} \sin\beta_{vis} \sin\beta_{IR} \chi^{(2)}_{zzz}
\end{aligned} \tag{2.11}$$

The Fresnel coefficients depend on the incident and emitted beam angles and refractive indices of the medium at the respective frequencies. As all these parameters are constant in the measurements taken for this thesis the Fresnel coefficients can be considered constant.

Equation 2.11 shows that $\chi^{(2)}_{eff,ssp}$ and $\chi^{(2)}_{eff,ppp}$ must be different due to the different number of contributing factors so the intensity of the polarization combinations must also be different.

$\chi^{(2)}_{eff}$ contains two types of contributions, a resonant part which is related to the adsorbed molecules on the surface and a non–resonant part which is from the high

order terms of the substrate and is usually frequency independent.

$$\chi^{(2)}_{eff} = \chi^{(2)}_{R} + \chi^{(2)}_{NR} \tag{2.12}$$

If the frequency of the IR beam does not excite any molecular vibrations of the molecules at the surface the $\chi^{(2)}_{R}$–term becomes zero and the signal will be dominated by the non–resonant term.

$\chi^{(2)}_{NR}$ can be described as follows with the amplitude A_{NR} and the phase ϕ_{NR}.

$$\chi^{(2)}_{NR} = |A_{NR}|e^{i\phi_{NR}} \tag{2.13}$$

Both values are fixed for a specific substrate as long as the experimental geometry stays the same.

If the frequency of the IR beam excites molecular vibrations $\chi^{(2)}_{R}$ of the resulting signal depends on the number of resonances q.

$$\chi^{(2)}_{R} = \sum_{q} \frac{|A_q|}{\omega_{IR} - \omega_q + i\Gamma} \tag{2.14}$$

A_q is the amplitude of the resonance q with the center frequency ω_q and the bandwidth Γ. Inserting equations 2.13 and 2.14 in equation 2.12 results in the macroscopic description of $\chi^{(2)}_{eff}$.

$$\chi^{(2)}_{eff} = \chi^{(2)}_{NR} + \sum_{q} \chi^{(2)}_{R} = |A_{NR}|e^{i\phi_{NR}} + \sum_{q} \frac{|A_q|}{\omega_{IR} - \omega_q + i\Gamma} \tag{2.15}$$

For a macroscopic description of the intensity of emitted SFG light equation 2.15 is inserted in equation 2.10.

$$I_{SFG} \propto \left| |A_{NR}|e^{i\phi_{NR}} + \sum_{q} \frac{|A_q|}{\omega_{IR} - \omega_q + i\Gamma} \right|^2 I_{vis} I_{IR} \tag{2.16}$$

The non–resonant contribution to the intensity is constant for *ssp* and *ppp* respectively. If the IR frequency excites molecular vibrations the resonant contribution is added to the constant non–resonant contribution and the overall signal intensity increases. This is shown in Figure 2.1.

SFG is a surface sensitive spectroscopy method like all $\chi^{(2)}$ processes. Nonlinear media can generally be split into two groups: media with and without inversion symmetry. Media with inversion symmetry e.g. centrosymmetric crystals have zero

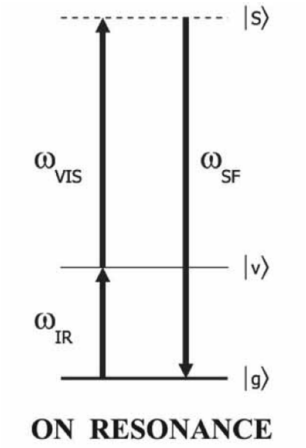

Figure 2.1.: SFG process on resonance [14]

bulk second–order susceptibility due to their symmetry.

The effect of a sign change of the incoming electric field on the induced polarization is shown in equations 2.17 and 2.18 [16].

$$P^{(2)} = \epsilon_0 \chi^{(2)} \cdot E_1(t) E_2(t) \tag{2.17}$$

$$-P^{(2)} = \epsilon_0 \chi^{(2)} \cdot \Big[- E_1(t) \Big] \Big[- E_2(t) \Big] \tag{2.18}$$

Both equations can only be fulfilled if $\chi^{(2)} = 0$. So all media with inversion symmetry generate no SFG. The vibration modes that are SFG active have to be both IR and Raman active [14]. A majority of bulk phases, for example the solution bulk are centrosymmetric, but the symmetry is broken at an interface. Therefore SFG is a surface sensitive spectroscopy method enabling the specific investigation of molecules adsorbed on a surface.

A metal surface has an additional influence on the SFG response. The presence of free electrons at the metal surface influences the vibrational spectrum due to the interaction of the electrons with the applied electric field of the laser creating an additional selection rule for SFG. If the transition dipole oscillates parallel to the surface the corresponding molecular vibration will not be visible in both SFG and IR reflection vibrational spectra [17]. The reason for this is the creation of an image dipole in the surface canceling the effective dipole of a molecular vibration as shown in Figure 2.2. The same process enhances the effective dipole of a molecular vibration perpendicular to the surface.

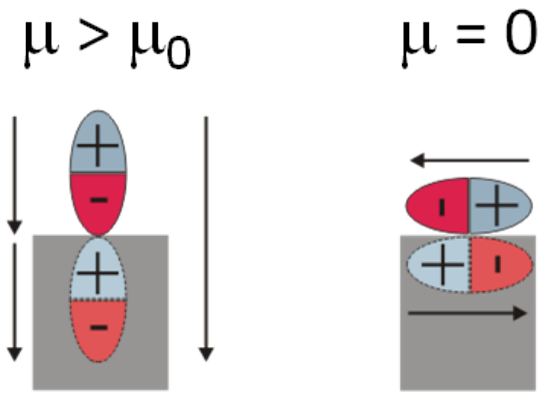

Figure 2.2.: Image dipole in a metal surface [17]

2.2. Cyclic voltammetry

Voltammetry is a widely used technique for acquiring qualitative information about electrochemical reactions. In this case it is the electro-oxidation of formic acid by electron transfer between molecule and electrode. Electrode reactions like this generally contain three steps: reactant movement to the electrode surface, electron transfer between electrode and reactant and movement of the product into the bulk phase. The number of flowing electrons during the electron transfer is the measured current.

The driving force of a reaction like this is the application of a potential. The unit of the potential

$$V = \frac{J}{C} \tag{2.19}$$

makes this clear as it defines potential as the energy required to move a charge. In nonmetals the electrons occupy discrete energy levels in the molecular orbitals providing a highest occupied molecule orbital (HOMO) and a lowest unoccupied molecule orbital (LUMO). Metal atoms in a metallic solid are closely packed forming a strictly periodic lattice. Therefore their atomic orbitals overlap strongly and the discrete electron energy levels become a continuum of energy levels filled with electrons. The highest occupied energy level in this continuum is called the Fermi level. This level is not fixed like a HOMO but can be altered by applying a potential to the electrode.

Electron transfer reactions at the electrodes only occur if they are thermodynamically favorable so from higher to lower energy levels. By applying a potential the Fermi level of the electrode electrons is altered until it is higher than the LUMO of the

reactant for a reduction or lower than the HOMO of the reactant for an oxidation (Figure 2.3). The electrode potential has not only an influence on the occurrence

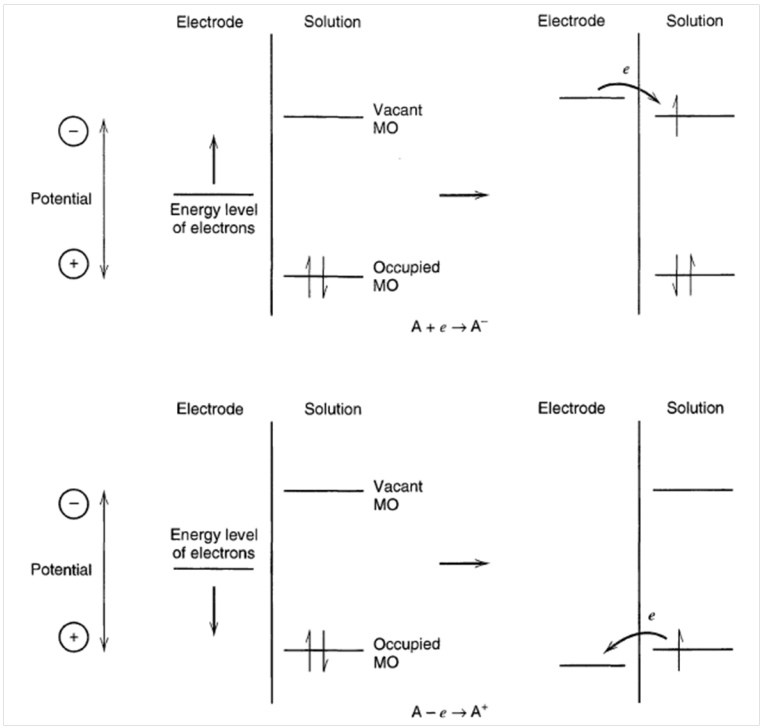

Figure 2.3.: Effect of applied potential on the fermi level and the reaction [18]

of the reaction but also on its kinetics. For developing a quantitative model of this influence a single electron transfer reaction between an oxidized species O and a reduced species R suffices.

$$O + ne^- \underset{k_{ox}}{\overset{k_{red}}{\rightleftharpoons}} R \tag{2.20}$$

An accurate kinetic description of a dynamic process has to form a thermodynamic equation in equilibrium. The equilibrium of electrode reactions is characterized by the Nernst equation.

$$E = E_0 + \frac{RT}{nF} \cdot \ln \frac{c_O^*}{c_R^*} \tag{2.21}$$

The equation links the electrode potential E to the bulk concentrations $c_{O,R}^*$ of the participating species. E_0 is the standard potential of the redox pair.

Considering the oxidation and reduction as individual reactions both processes proceed at a certain rate $\nu_{ox,red}$. This rate is proportional to the produced current and can be described by the rate constant $k_{ox,red}$ and the surface concentration $c_{O,R}$[18].

$$\nu_{ox,red} = k_{ox,red} \cdot c_{O,R} = \frac{i_{a,c}}{nFA} \tag{2.22}$$

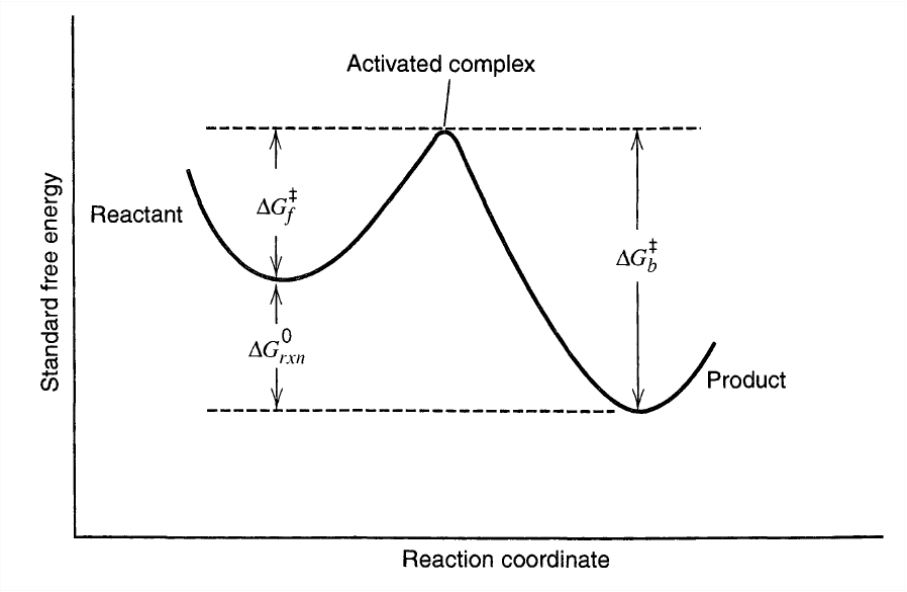

Figure 2.4.: Free energy profile of the reaction. The activated complex (transition state) is the configuration of maximum free energy [18]

The reduction produces a cathodic current i_c while the oxidation produces an anodic current i_a both being components of the total current i.

The total current is determined by the difference of its cathodic and anodic components.

$$i = i_c - i_a = nFA\left(k_{red}c_O - k_{ox}c_R\right) \tag{2.23}$$

Using the transition state theory the influence of the applied potential on the rate constants can be established [18]. In this theory the reaction proceeds via an energy barrier ΔG the transition state being the summit of said barrier. This barrier height represents the activation energy of the reaction.

The kinetics of the reaction can be described by the Arrhenius equation like most solution–phase reaction kinetics.

$$k_{ox,red} = Z \cdot \exp\left(\frac{-\Delta G}{k_B T}\right) \tag{2.24}$$

Z is the frequency factor divided by the constant exponential of the standard entropy of activation representing the frequency of attempts to overcome the activation barrier while the exponential factor represents the probability of surmounting the energy barrier using thermal energy [18].

The free energy profile shown in Figure 2.4 changes depending on the applied potential. In equilibrium the reaction rates of oxidation and reduction are the same and both

sides have the same free energy. Applying a potential alters the Fermi level of the metal electrons and thus also the free energy of the reduction and oxidation products. In the free energy profile this is shown by lowering one side and heightening the other resulting in a change of the overall activation barrier. This favors either the oxidation or reduction depending on the potential. The two reactions are no longer in equilibrium so their rate constants become different. Assuming a linear relationship between the applied potential and the free energy change the activation free energies of oxidation and reduction can be described by the Butler–Volmer model [18].

$$\Delta G_{red} = \Delta G_{red,0} + \alpha FE \tag{2.25}$$

$$\Delta G_{ox} = \Delta G_{ox,0} - (1-\alpha)FE \tag{2.26}$$

E is the applied potential and $\Delta G_{ox,red,0}$ are the activation energies in equilibrium ($E = 0$). The parameter α is the transfer coefficient which can range from zero to unity. Inserting equations 2.25 and 2.26 in equation 2.24 results in a potential dependent expression for the rate constants.

$$k_{red} = Z \cdot \exp\left(\frac{-\Delta G_{red,0}}{k_B T}\right) \cdot \exp\left(\frac{-\alpha FE}{k_B T}\right) \tag{2.27}$$

$$k_{ox} = Z \cdot \exp\left(\frac{-\Delta G_{ox,0}}{k_B T}\right) \cdot \exp\left(\frac{-(1-\alpha)FE}{k_B T}\right) \tag{2.28}$$

This shows that the rate of the reaction can be altered by simply changing the applied potential.

In addition to the reaction rate the overall reaction is also influenced by the rate of molecule transport to the electrodes. Mass transport in an electrochemical cell consists mainly of diffusion. Diffusion is the process of leveling out local concentration differences and is responsible for transporting reactants and products from and to the electrode. The higher the difference the faster the molecule transport occurs. When the electron reaction rate at the electrode is so high that all reactant in reach is immediately turned to product the overall reaction is mass transport limited.

There are different voltammetry techniques which can each give different information about the reaction. The most important technique for this thesis is cyclic voltammetry. In cyclic voltammetry experiments the potential is swept from a low potential to a higher one with a defined scan rate. After reaching the higher potential the process is reversed completing the cycle. The measured current is plotted versus the applied potential. The resulting graph is a cycle like the one shown in Figure 2.5.

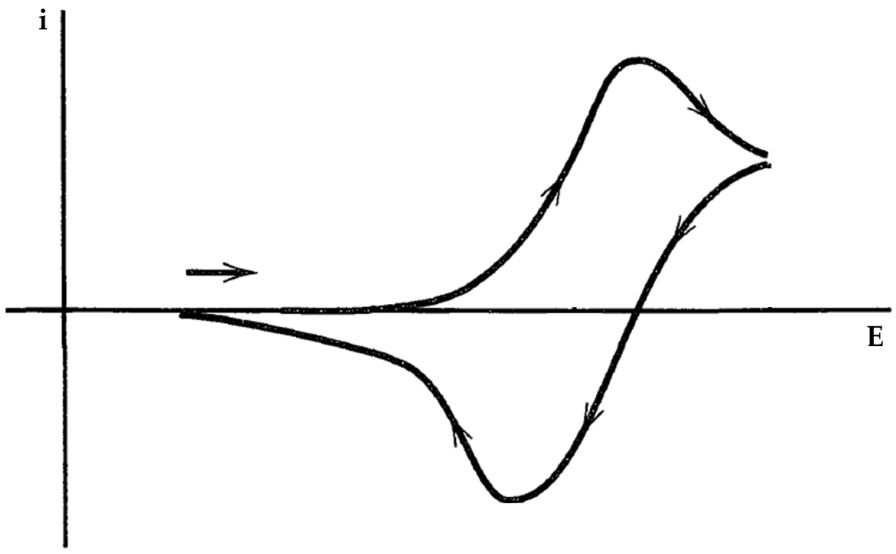

Figure 2.5.: Cyclic voltammogram for a reversible electron transfer reaction

For reversible electron transfer reactions the cyclic voltammogram (CV) has two peaks – an oxidation and a reduction peak. Peaks occur because at that potential the electrode reaction is much faster than the diffusion rate. In front of the electrode the product forms a layer. This diffusion layer impedes the diffusion of new reactant to the electrode resulting in a current drop and the above mentioned peak. In a reversible reaction this process is repeated for the backward sweep. Another reason for peaks is the formation of an adsorption layer on the electrode. The adsorbed molecules block the available space on the electrode also resulting in a current drop. Distinguishing between these two peaks is possible using Potential Step Voltammetry.

In potential step experiments the potential is applied stepwise with jumps from one potential to the other. During the experiment the current is recorded versus the time. If an electrode reaction occurs at the applied potential the current increases in the beginning. Then it either becomes a stable plateau or it decreases again. If the current becomes stable the electrode reaction is not fast enough to be mass transport limited. If it decreases the reaction is mass transport limited at the applied potential. When doing potential steps with peak potentials from a CV a decreasing current indicates an oxidation or reduction while a stable current indicates an adsorption.

3. Experimental Methods

3.1. Experimental setup

For spectroelectrochemistry with SFG the electrochemical cell was installed in a SFG laser setup. The laser in question is a Ti:sapphire laser which is a widely used solid–state laser. The 800 nm pulses from the Ti:sapphire oscillator (Vitesse: Coherent, Inc.) were amplified to a pulse length of 50 fs at 1000 Hz with a pulse energy of about 8 mJ. The HE Topas (Light Conversion) was pumped with 5 mJ providing tunable IR pulses with a pulse duration of 55 fs and a pulse energy of 24—28 µJ at 4 µm. The remaining 800 nm pulse from the OPA process was sent to a home made pulse shaper to generate the narrow band visible up–conversion pulse (about 3 ps).

The electrochemical cell in question was a thin–film cell consisting of a bottom part holding a glass plate with vapor deposited gold electrodes and an upper part with a magnesium fluoride window and metal tubes for connecting the cell to a pump (Figure 3.1). The cell was assembled with a 50 µm Teflon spacer and a bubble free liquid film of the used electrolyte in between the two parts.

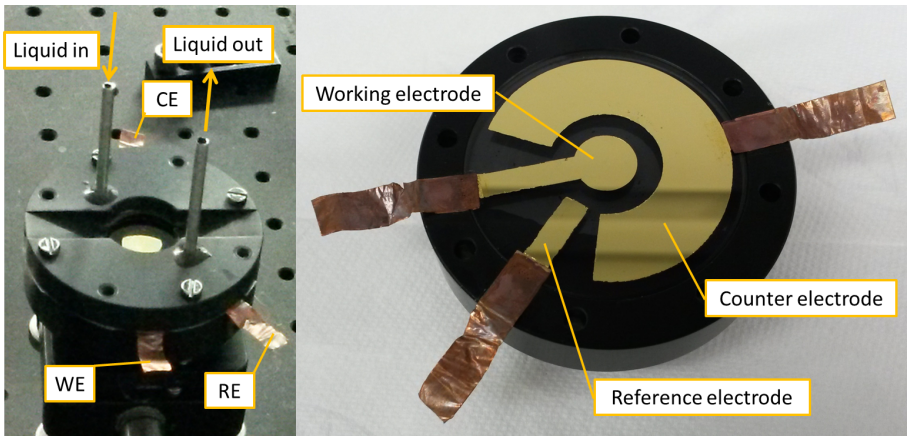

Figure 3.1.: Electrochemical thin–film cell. Completely assembled cell on the left and bottom part with vapor deposited gold electrodes on the right.

The electrochemical cell was installed in the setup with both the visible and IR beam focused on the working electrode (Figure 3.2) and the resulting SFG was then directed to the detector – a spectrometer dispersing the signal via a grating (1200 g/mm) across a ICCD camera (Princeton Instruments). The pulse energy of both beams was adjusted to about 3 µJ so the gold surface of the working electrode was not damaged.

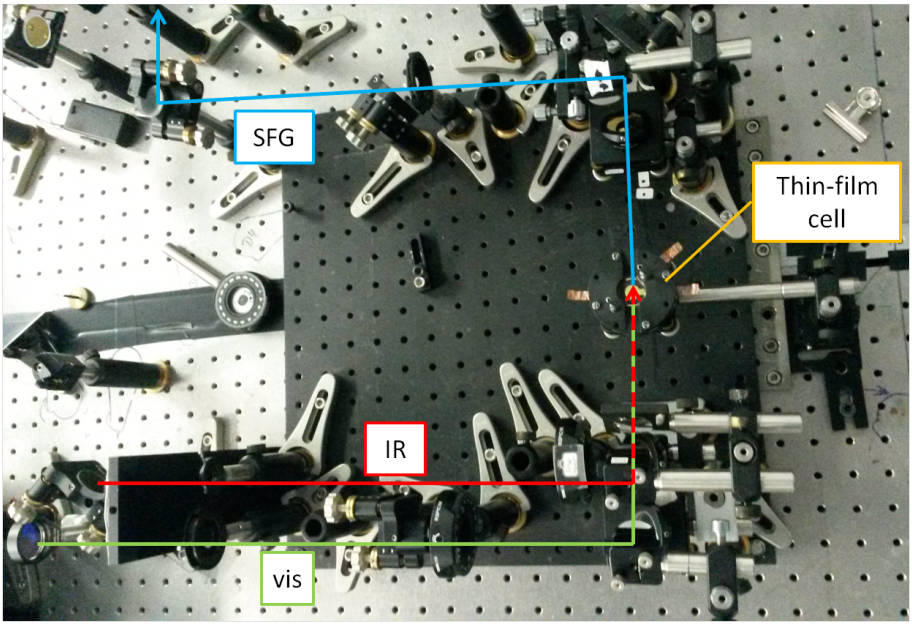

Figure 3.2.: Laser setup surrounding the electrochemical thin–film cell. For clarity the tubes for pumping the liquid and the wires to the potentiostat are not shown.

Before the measurement the SFG signal was optimized. This was done by optimizing the temporal and spatial overlap of the beams. After signal optimization the cell was connected to the liquid pump and the potentiostat. The pump was used to ensure a steady electrolyte flow across the electrodes with a flow rate of about 29 µl/s using a electrolyte reservoir. This was used for bubbling the electrolyte with nitrogen so that the liquid remained oxygen free.

3.2. Data acquisition

Before the actual measurement of SFG spectra during the electrochemical experiment a few additional spectra were taken. These were necessary for the data analysis later. At first a spectrum of either quartz or gold with a magnesium fluoride window on top was taken. This was necessary for determining the spectral shape of the IR beam.

Then a spectrum of a neon lamp directly in front of the detector was taken to be able to match the pixel positions in the camera to the corresponding frequencies.

After installing the cell and optimizing the signal a spectrum at open circuit (no applied potential) was taken. This shows later the situation on the surface without any applied potential.

The CV experiment was started by doing a few fast cycles (50 mV/s) to clean the electrode surface of possibly adsorbed molecules. When using the electrode plate for the first time this was done in 0.5 M sulfuric acid instead of the used electrolyte. Then continuous spectra are taken while scanning the potential. This was done for the polarization combinations *ppp* and *ssp*, respectively. The used electrolyte was 0.1 M perchloric acid in D_2O or H_2O and the process was repeated for the same solution additionally containing 1 M formic acid . With the formic acid electrolyte additional spectra were taken while doing potential steps at relevant potentials (−0.1 V, 0.4 V, 0.9 V, 1.2 V and 1.5 V).

This data acquisition was done for the IR center frequencies 3.4 µm, 6.2 µm and 7.1 µm. At 7.1 µm the solution was done with normal deionized water instead of D_2O. For 6.2 µm a box around the SFG setup containing the cell was flushed with nitrogen to prevent absorption bands of water vapor in the air. For all the above mentioned spectra background spectra were taken by blocking a beam. The recorded CVs and SFG spectra were processed using Igor Pro (Wavemetrics). Before further analysis all spectra were background subtracted and normalized by the IR shape spectrum taken on quartz or gold.

4. Data Analysis

4.1. Electrochemistry

The first thing to do when analyzing an electrochemical reaction is to examine the cyclic voltammogram. The cyclic voltammograms from the base solution (0.1M $HClO_4$ in D_2O) and the formic acid solution (1M HCOOH + 0.1M $HClO_4$ in D_2O) are shown in Figure 4.1 and 4.2.

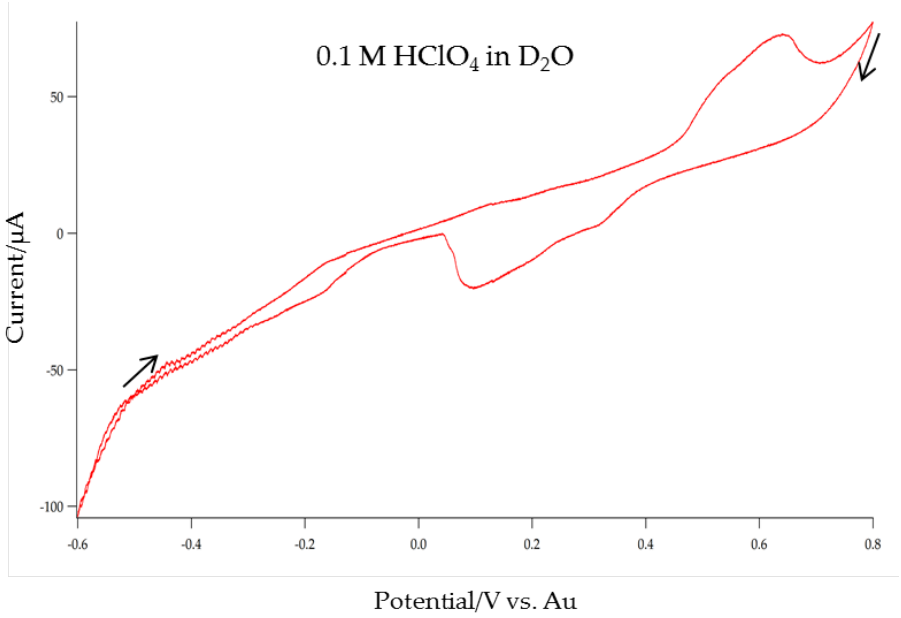

Figure 4.1.: Cyclic voltammogram of the base solution

Both CVs have one oxidation and reduction peak, respectively. The main difference is the potential range. The potential range for each CV was determined by testing different ranges to get the maximum range without gas production. Gas production was avoided due to the difficulties of SFG spectroscopy with bubbles on the working electrode. Testing different ranges was necessary because the potentials could not be compared to literature as the gold reference electrode defining the potential is not a standard reference electrode like Hg/Hg_2SO_4. The use of a standard reference

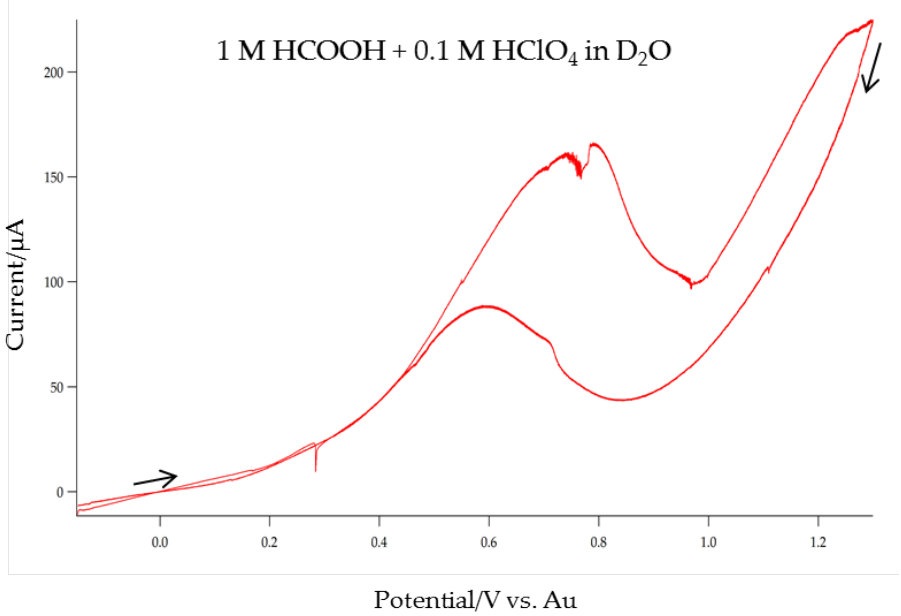

Figure 4.2.: Cyclic voltammogram of the solution containing formic acid

electrode was not possible as all electrodes had to be vapor deposited on the glass plate.

Even though the base solution does not contain electroactive species it has both an oxidation and reduction peak. The oxidation peak can be either a real oxidation peak or an adsorption peak as mentioned in the theoretical concepts. In this case it is most likely an adsorption peak due to the adsorption of OD on the surface because an oxidation would result in gas production. If even higher potentials would be applied the gold surface would be oxidized and the real oxidation peak would be visible in the CV.

The formic acid solution on the other hand contains an electroactive species. If the visible peak is an adsorption peak or an oxidation peak depends on the reaction mechanism. As proposed by Hamelin et al. [8] the electrooxidation mechanism of formic acid has two possible pathways. The direct or formate pathway via adsorbed formate and the indirect pathway with oxidation via adsorbed carbon monoxide. On gold they found that only the direct pathway without formation of adsorbed CO occurs. This indicates that the visible peak is an adsorption peak and the oxidation to CO_2 occurs at higher potentials. The lack of gas production at the peak potential supports this assumption.

Testing if the peak is an adsorption or oxidation peak was done by doing potential steps at several potentials and comparing the current development, respectively. This

is shown in Figure 4.3.

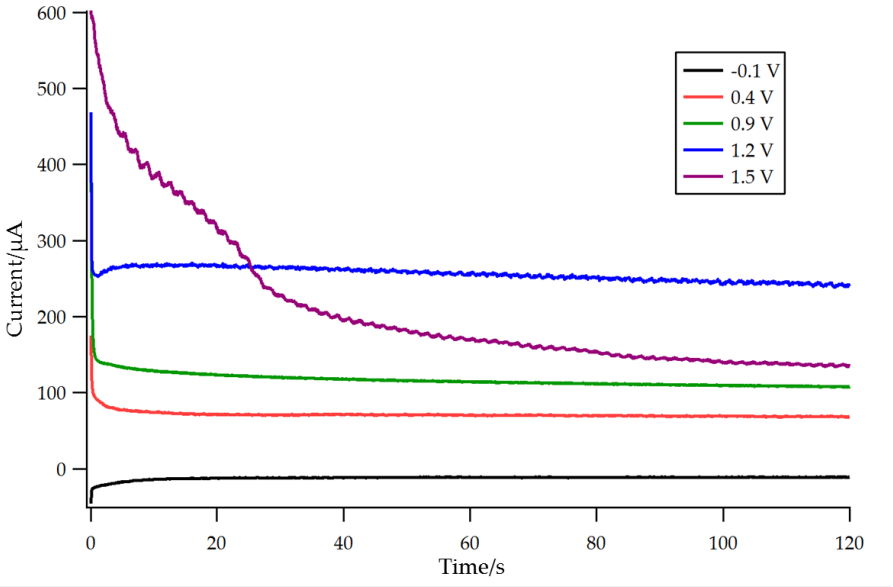

Figure 4.3.: Potential Step experiment. The current stays stable until 1.2 V, then it starts to decrease. This shows the current peak in the CV at about 0.8 V is an adsorption peak and no oxidation peak.

The current stays stable at the potentials −0.1 V, 0.4 V, 0.9 V and 1.2 V and decreases over time at 1.5 V. This shows that the peak at around 0.8 V in the CV is indeed an adsorption peak instead of an oxidation peak as applying the oxidation potential results in decreasing current over time.

So a species adsorbs on the surface with increasing potential until the reaction becomes mass limited and the current decreases. Then the potential decreases and the species desorbs from the surface. By driving the potential to higher values it would be possible to see the oxidation peak and the resulting gas production due to the formation of CO_2.

As mentioned before this adsorbed species is widely believed to be adsorbed formate. For more information about the adsorbed species SFG spectra were taken during the CVs.

4.2. SFG

Previous studies proposed two possible adsorption geometries which are shown in Figure 4.4. Using SFG spectroscopy this argument can be concluded.

(a) adsorbed HCOO (b) adsorbed COOH

Figure 4.4.: Schematic drawings of possible adsorbate geometries on the gold surface (thick line)

Bridge-bonded formate adsorbs on the surface with its C–H bond perpendicular to the surface (Figure 4.4a) while hydroxylcarbonyl adsorbes to the surface with its carbon atom (Figure 4.4b).

If the adsorbed species is bridge–bonded formate the C–H stretch should be visible in the 3000 cm^{-1} region, so the first spectra were taken with an IR center frequency of 3.4 µm (2940 cm^{-1}). For seeing the potential dependent changes spectra were taken every 100 mV while scanning the potential with 5 mV/s (Figure A.1–A.4). This was done with both solutions and the direct comparison of both spectra (*ppp* polarization) at open circuit potential is shown in Figure 4.5. The spectra were also taken in

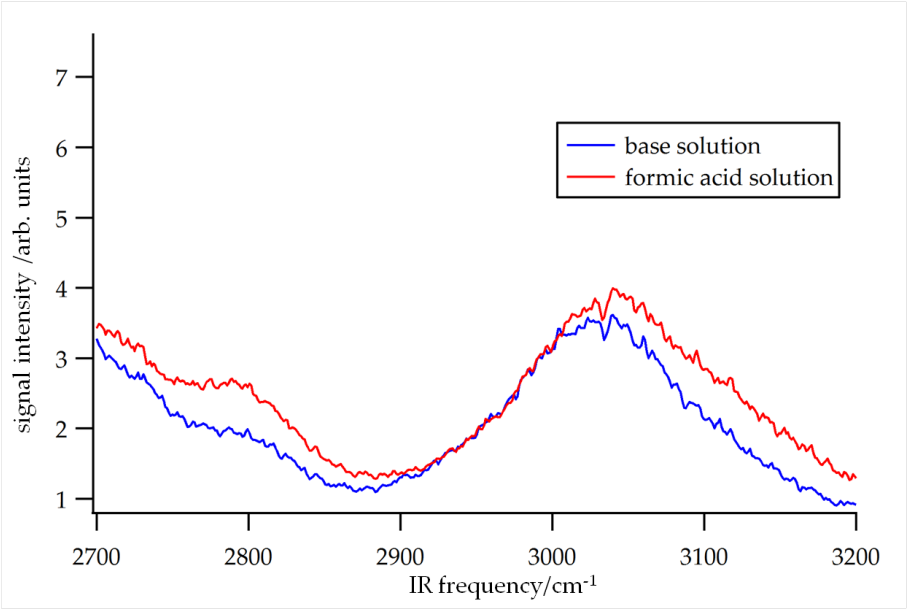

Figure 4.5.: Direct comparison of SFG spectra at 3.4 µm (IR frequency) with *ppp* polarization.

ssp polarization (Figure A.5 and A.6) but as the features stay the same and just the signal intensity is lower the following analysis will be done only with the *ppp* polarized spectra.

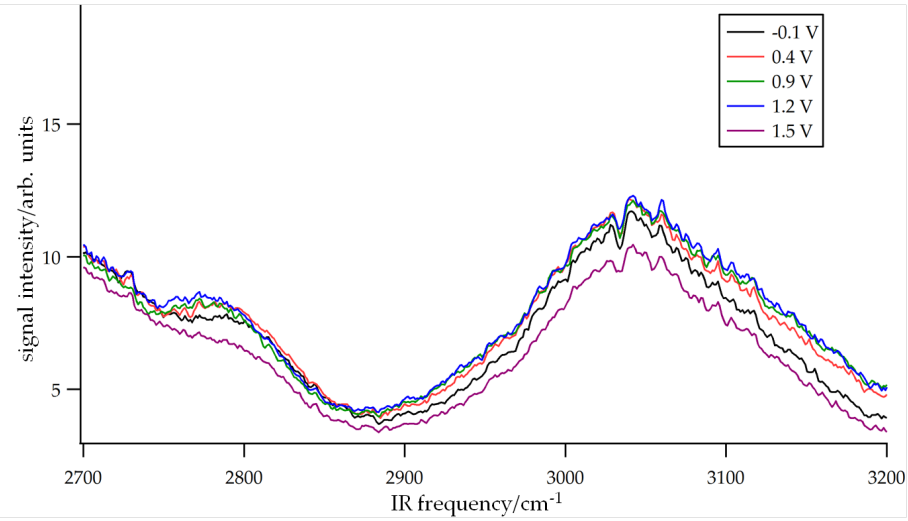

Figure 4.6.: Formic acid spectra at different potentials showing the potential dependence of the features. These spectra were taken during the potential step experiment.

The signal of the base solution is purely the non–resonant signal from the gold substrate. The frequency dependent features visible can be understood as the absorption of IR by the bulk D_2O of the thin layer. The formic acid spectrum has similar features which are potential dependent as is shown in Figure 4.6. The similarity of the features shows strong interference effects between the frequency dependent non–resonant signal and the resonant signal.

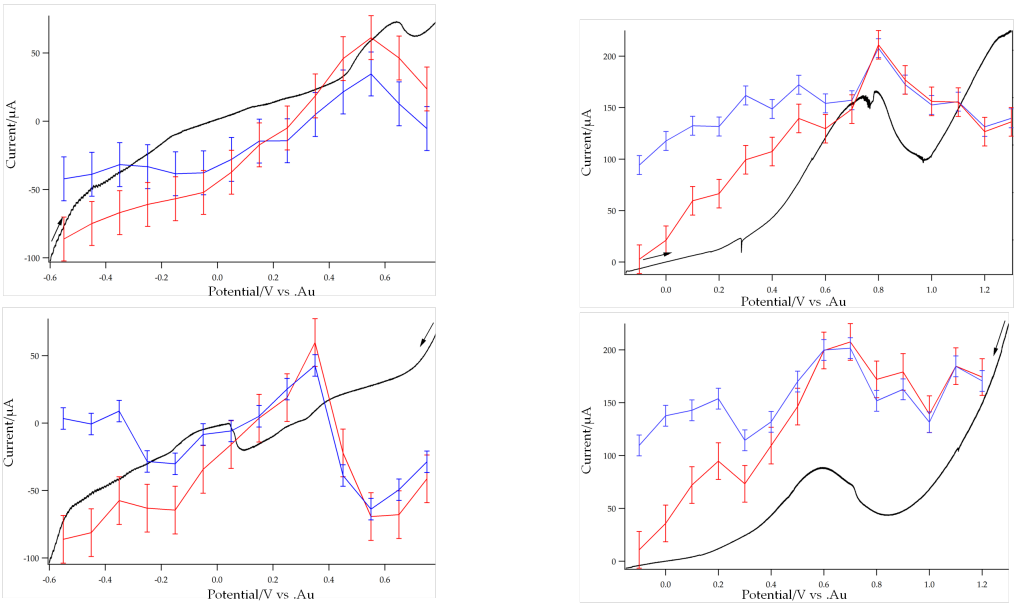

(a) Base solution (b) Formic acid solution

Figure 4.7.: Integrated peak intensities (blue: $2800\,\mathrm{cm}^{-1}$, red: $3000\,\mathrm{cm}^{-1}$) in direct comparison with the CV (black). The error bars are estimated by comparing the integrated intensities of two cycles.

Due to this complicated effects the peak center frequency and bandwidth of the resonant signal are not clear but the potential dependent features are quite obvious. To see these features more clearly the contribution of formic acid has to be isolated. For achieving this the features of both solutions were integrated and plotted against the potential, respectively. Figure 4.7 shows the potential dependence of the features' integrated intensity in direct comparison to the respective CVs. The potential dependence of the base solution shows the surface change during the CV with a maximum intensity at the potential of the adsorption peak in the CV. The potential dependence of the formic acid solution shows the surface change and in addition the change due to formic acid. By comparing the intensity change of both solutions and matching the potentials accordingly, the formic acid spectra were normalized using the base solution spectra. This was done for four different potentials and is shown in Figure 4.8. For better visibility the curves were smoothed.

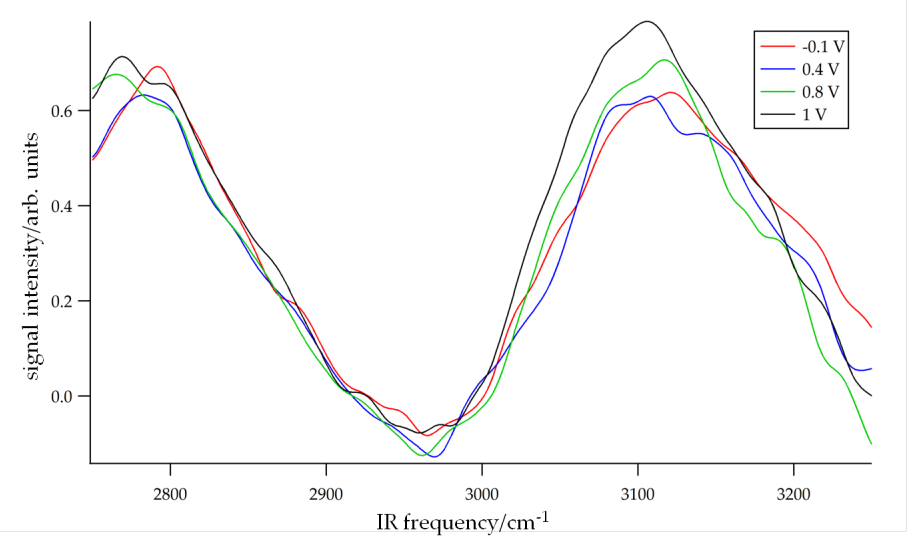

Figure 4.8.: Direct comparison of formic acid solution spectra normalized by base solution spectra at four different potentials.

The visible features in the normalized spectra are solely related to the reaction intermediates. The feature at2750 cm^{-1} is adsorbed OD and the feature at 3100 cm^{-1} is the C–H stretch of the adsorbed formate. This confirms the findings of others [19, 11, 12] that bridge–bonded formate is adsorbed at the surface during the oxidation of formic acid. The question if it is the active intermediate or just a spectator is answered by the potential dependence of this feature shown in Figure 4.6. It corresponds well to the CV with an increasing intensity until a certain potential and a decreased intensity at 1.5 V, which was confirmed before to be an oxidation potential. This indicates that the adsorbed formate is indeed an active intermediate

and is oxidized to carbon dioxide at this potential. However, due to the complicated spectral line shapes, it is impossible to separate the pure resonances.

In order to confirm that the reaction intermediate is indeed formate, we have also measured spectra in the low frequency region with an IR center frequency of 7.1 µm (1410 cm^{-1}) because the formate band is at about 1350 cm^{-1}. The spectra were taken every 150 mV while scanning the potential with 0.5 mV/s. As the aim of this measurement was just to observe the formate band and verify that it is potential dependent, the measurement was done only with the formic acid solution (see Figure A.7 and A.8). In addition spectra were taken during a potential step experiment to better show the potential dependence (Figure 4.9).

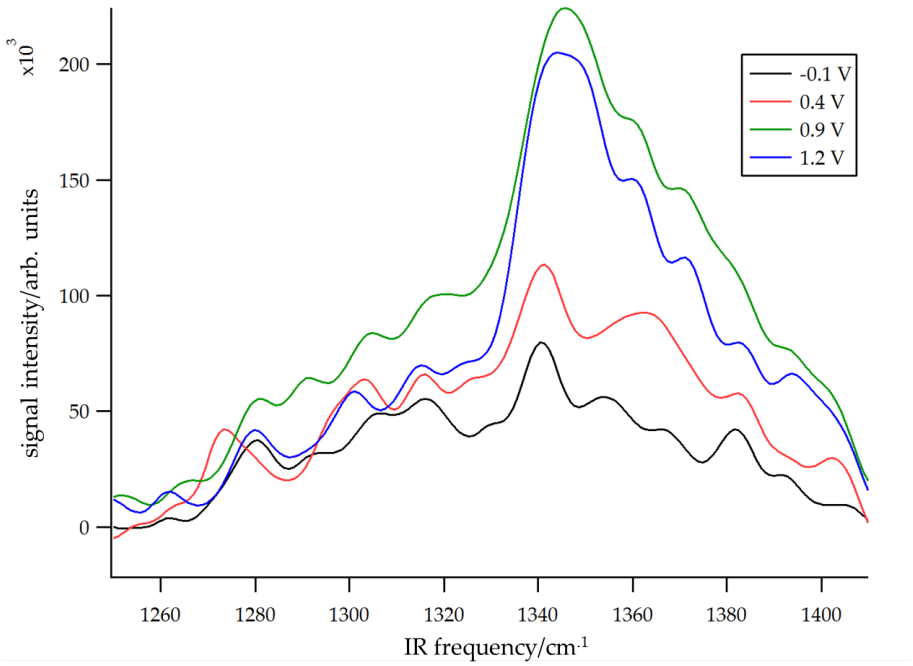

Figure 4.9.: Formic acid spectra at different potentials showing the potential dependence of the formate band. The curves were smoothed for better visibility.

The intensity of the formate band increases with the potential until it decreases between 0.9 V and 1.2 V. This verifies the existence of adsorbed formate at the surface during the oxidation. The potential dependence reveals the increasing coverage until potentials high enough for an oxidation and a subsequent decrease of coverage confirming bridge–bonded formate to be the active intermediate of the oxidation.

If the adsorbate in the other geometry (Figure 4.4b) also exists, the CO stretch would be visible at about 1750 cm^{-1}. So we measured spectra with an IR center frequency of 6.2 µm (1620 cm^{-1}) every 85 mV while scanning the potential with 2.5 mV/s. The

spectra were taken with both solutions. The direct comparison of both solutions at open circuit potential showed that the one from the formic acid solution is similar to the one from the base solution except one dip in the 1700 cm^{-1} region (see Figure A.9). Matching the spectra according to their intensities the formic acid spectra were normalized using the base solution spectra. This was done for five potentials and is shown in Figure 4.10.

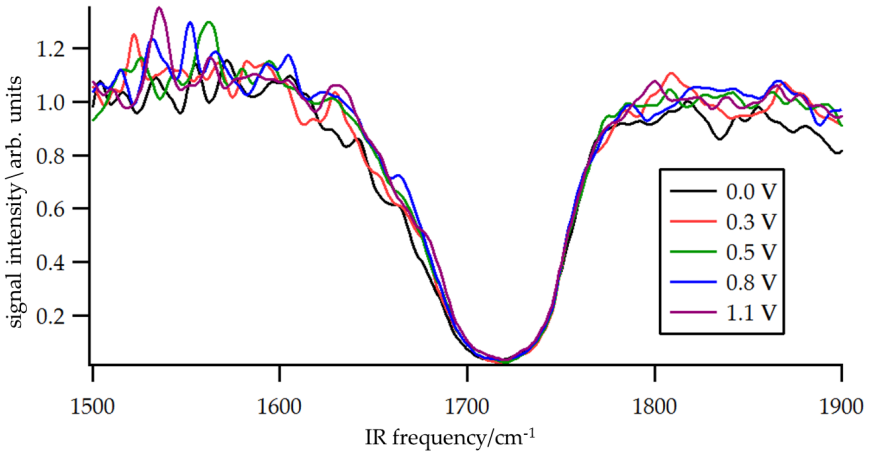

Figure 4.10.: Formic acid spectra in the 1700 cm^{-1} region. All spectra were normalized by the base solution spectra and smoothed for better visibility.

The dip is not potential dependent because it is not the signal of a CO stretch of adsorbed formate but the absorption of IR in the formic acid solution. This explains the dip instead of a peak, because the IR is missing in this region and not exciting resonances generating SFG. Due to this adsorption a possible C=O bond cannot be excited so it is not possible to say if adsorbed hydroxylcarbonyl in the geometry shown in Figure 4.4b is also present on the surface. The same applies to the existence of adsorbed formic acid.

5. Summary and Outlook

The purpose of this thesis was to gain further insight into the electrooxidation mechanism of formic acid on transition metal electrodes. For this the surface adsorbates were probed during cyclic voltammetry and potential step experiments using SFG.

The analysis of the cyclic voltammograms showed that the CV of the electrooxidation of formic acid has two peaks. The first one around 0.8 V is the adsorption peak of the accumulating formate on the surface while the second one is the oxidation peak of the oxidation to CO_2 and is at potentials higher than 1.3 V. The potential in the experiments was not scanned further than 1.3 V to avoid gas production hindering the SFG measurements.

Two different geometries for adsorbates during the electrooxidation of formic acid on gold were previously proposed. To confirm the assumed bridge–bonded geometry of adsorbed formate the 3000 cm^{-1} region was probed aiming to observe a potential dependent C–H stretch. The observed feature at 3100 cm^{-1} was assigned to this C–H stretch and its potential dependence showed that bridge–bonded formate accumulates on the surface until a certain potential and is oxidized at higher potentials to CO_2 leaving the surface. This supports the information gained from the CV.

Confirming that the observed C–H stretch belongs to adsorbed formate was done by probing the 1400 cm^{-1} region. At 1350 cm^{-1} the potential dependent formate band was observed. The potential dependence was similar to the one of the C–H stretch confirming it belongs to bridge–bonded formate and that bridge–bonded formate is the active intermediate of the oxidation.

Probing the 1700 cm^{-1} was supposed to bring insight into the existence of another possible adsorbate. This could be either the other proposed adsorbate COOH or adsorbed HCOOH. Unfortunately the IR was absorbed by the solution at about 1700 cm^{-1} making it impossible to gain any insight in the possible adsorption of either adsorbate.

Based on this results a mechanism for the direct pathway of the formic acid electrooxidation on gold can be formulated.

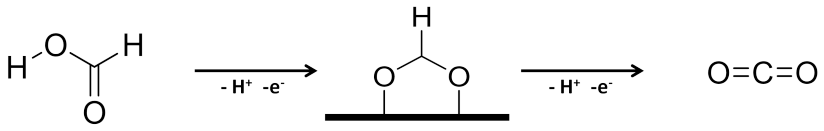

Figure 5.1.: Mechanism of the electrooxidation of formic acid on gold based on the results in this thesis.

This is just a first insight. Already the successful probing of the 1700 cm^{-1} region would give more information about different adsorbates and if the initial adsorption is a physisorption of formic acid or as suggested above a chemisorption of formate. Also measurements with different beam polarizations and experimental geometries can provide further information about the adsorption geometries. Furthermore doing the same measurements on platinum electrodes can maybe answer the question if the electrooxidation has the same mechanism on both metals, which was already theoretically evaluated by Gao et al. [12].

A. Measurements

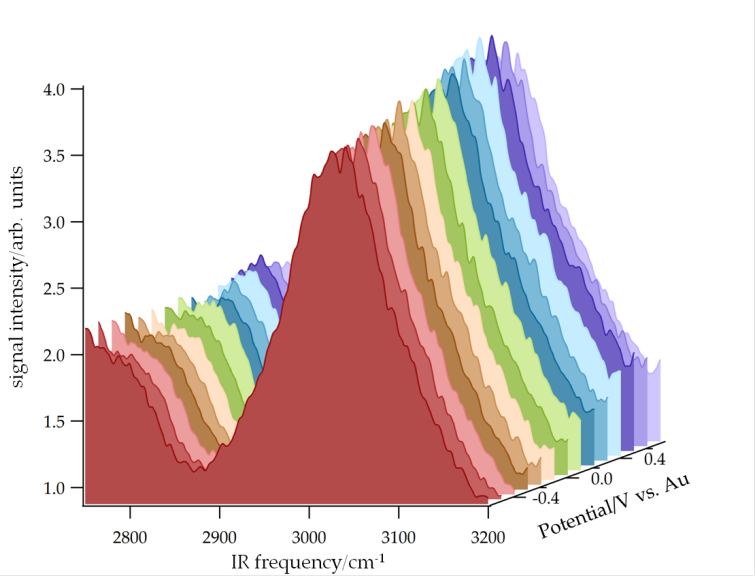

Figure A.1.: Spectra during the forward scan of the base solution (*ppp*)

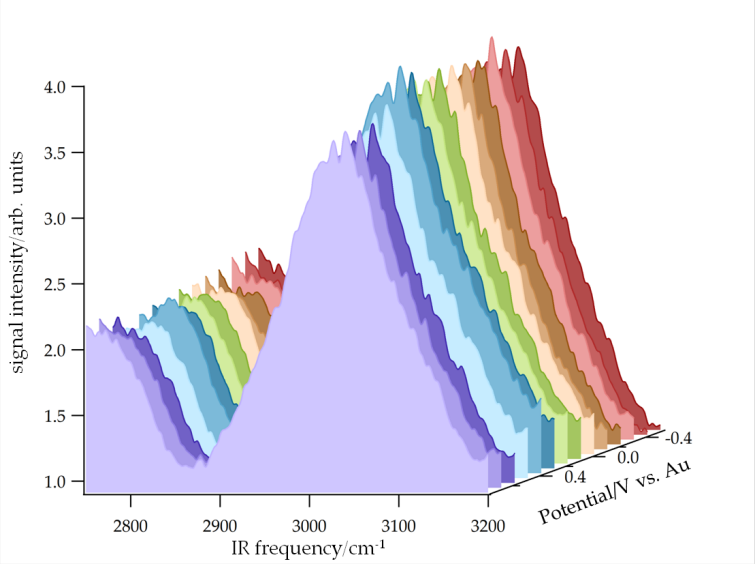

Figure A.2.: Spectra during the backward scan of the base solution (*ppp*)

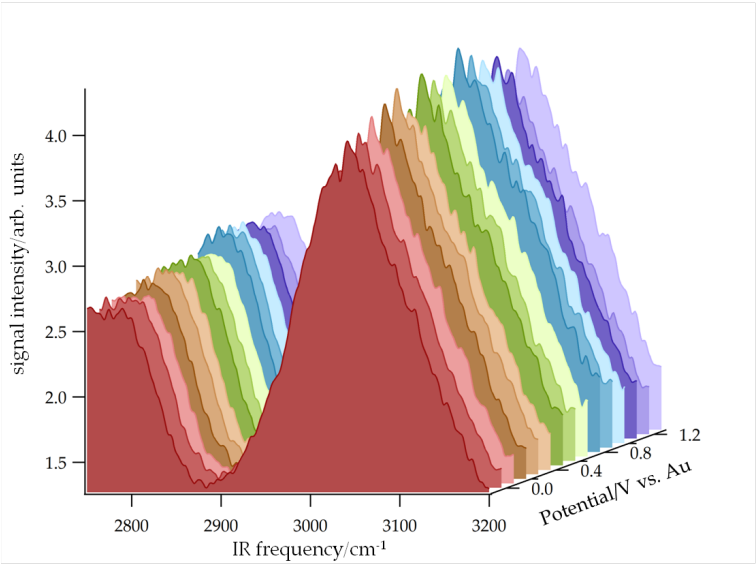

Figure A.3.: Spectra during the forward scan of the formic acid solution (*ppp*)

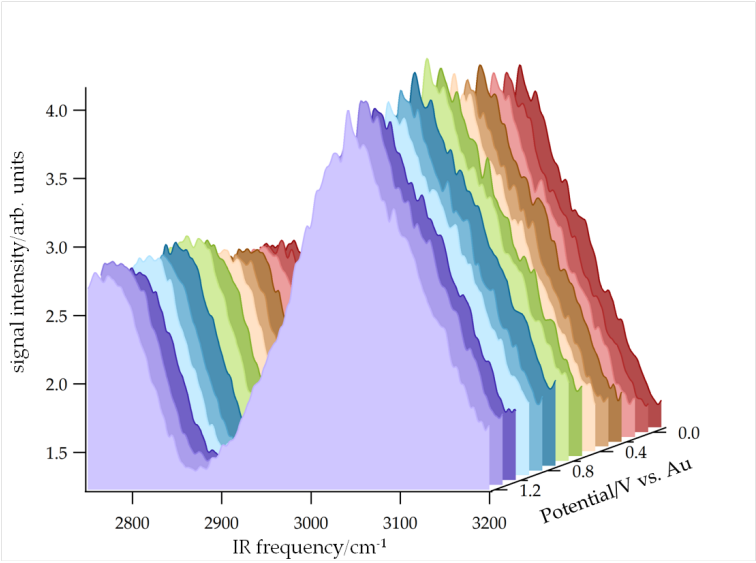

Figure A.4.: Spectra during the forward scan of the formic acid solution (*ppp*)

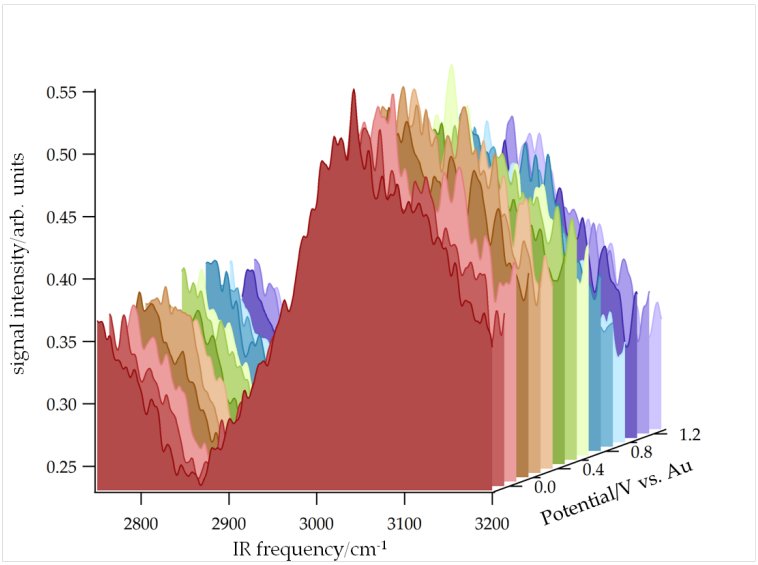

Figure A.5.: Spectra during forward scan of the formic acid solution (*ssp*)

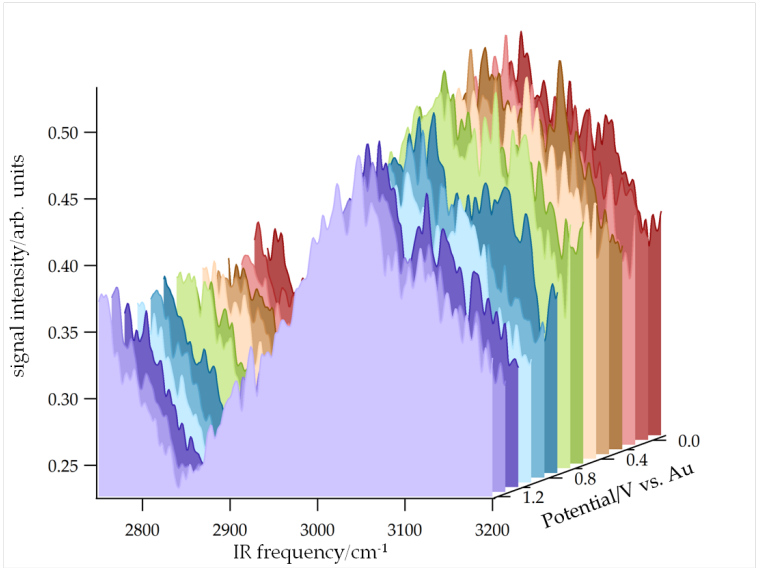

Figure A.6.: Spectra during the backward scan of the formic acid solution (*ssp*)

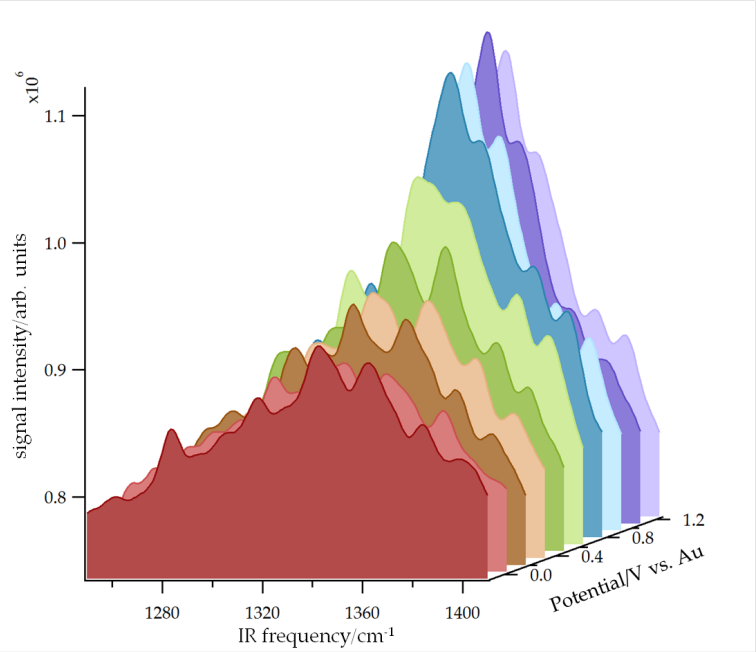

Figure A.7.: Potential dependence of the formate band during the forward scan of the formic acid solution (*ppp*)

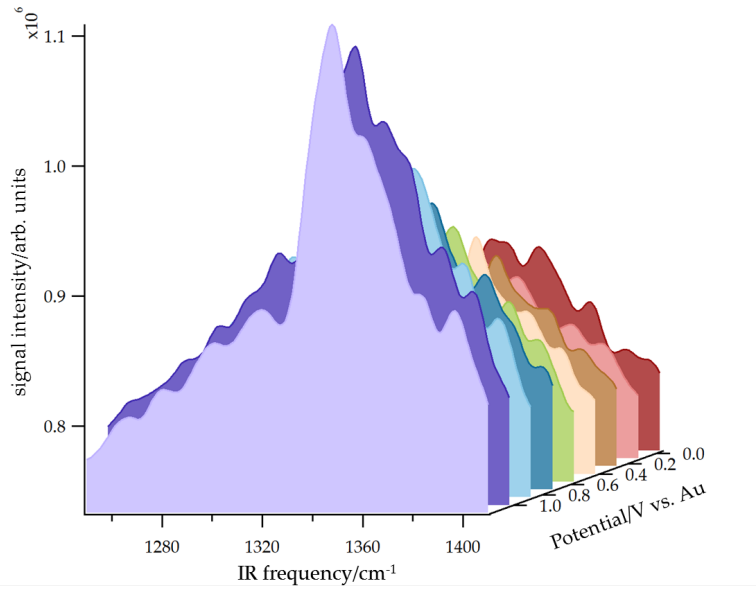

Figure A.8.: Potential dependence of the formate band during the backward scan of the formic acid solution (*ppp*)

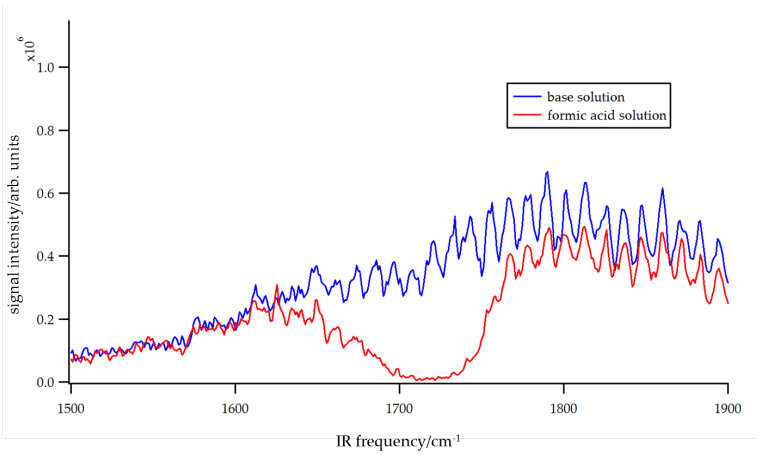

Figure A.9.: Direct comparison of the base solution and formic acid solution spectra in the 1700 cm^{-1} region.

Bibliography

[1] E. Müller *Z. Elektrochem.*, vol. 29, pp. 264–274, 1923.

[2] T. R. Ralph, "Proton Exchange Membrane Fuel Cells," *Platinum Metals Rev.*, vol. 41, pp. 102–113, 1997.

[3] W. Vielstich and H. A. Gasteiger, *Handbook of Fuel Cells*. Wiley, New York, 2003.

[4] A. Arico, S. Srinivasan, and V. Antonucci, "DMFCs: From Fundamental Aspects to Technology Development," *Fuel Cells*, vol. 1, pp. 133–161, 2001.

[5] X. Yu and P. G. Pickup, "Recent advances in direct formic acid fuel cells (DFAFC)," *J. Power Sources*, vol. 182, pp. 124–132, 2008.

[6] M. W. Breiter, "A study of intermediates adsorbed on platinized-platinum during the steady-state oxidation of methanol, formic acid and foraldehyde," *J. Electroanal. Chem.*, vol. 14, pp. 407–413, 1967.

[7] A. Capon and R. Parsons, "The oxidation of formic acid at noble metal electrodes Part III. Intermediates and mechanism on platinum electrodes," *J. Electroanal. Chem.*, vol. 45, pp. 205–231, 1973.

[8] A. Hamelin, Y. Ho, S. C. Chang, G. Xiaoping, and M. J. Weaver, "Surface crystallographic dependence of voltammetric oxidation of polyhydric alcohols and related systems at monocrystalline gold–acidic aqueous interfaces," *Langmuir*, vol. 8, pp. 975–981, 1992.

[9] A. Miki, S. Ye, and M. Osawa, "Surface–enhanced IR absorption on platinum nanoparticles: and application to real–time monitoring of electrocatalytic reactions," *Chem. Commun.*, pp. 1500–1501, 2002.

[10] G. L. Beltramo, T. E. Shubina, and M. T. Koper, "Oxidation of Formic Acid and Carbon Monoxide on Gold Electrodes Studies by Surface-Enhanced Raman Spectroscopy and DFT," *ChemPhysChem*, vol. 6, pp. 2597–2606, 2005.

[11] A. Cuesta, G. Cabello, F. Hartl, M. Escudero-Escribano, C. Vaz-Dominguez, L. Kibler, M. Osawa, and C. Gutierrez, "Electrooxidation of formic acid on gold:

An ATR-SEIRAS study of the role of adsorbed formate," *Catal. Today*, vol. 202, pp. 79–86, 2013.

[12] W. Gao, E. H. Song, Q. Jiang, and T. Jacob, "Revealing the Active Intermediates in the Oxidation of Formic Acid on Au and Pt (111)," *Chem. Eur. J.*, vol. to be published, 2014.

[13] P. Magnan, "Detection of visible photons in CCD and CMOS: A comparative view," *Nucl. Instrum. Methods Phys. Res., Sect. A*, vol. 504, no. 1, pp. 199–212, 2003.

[14] A. G. Lambert, P. B. Davies, and D. J. Neivandt, "Implementing the Theory of Sum Frequency Generation Vibrational Spectroscopy: A Tutorial Review," *Applied Spectroscopy Reviews*, vol. 40, pp. 103–145, 2005.

[15] H. Kirsch, J. Wirth, Y. Tong, M. Wolf, P. Saalfrank, and R. K. Campen, "Experimental Characterization of Unimolecular Water Dissociative Adsorption on α-Alumina," *J. Phys. Chem.*, vol. 118 (25), pp. 13623 –13630, 2014.

[16] H. Arnolds and M. Bonn, "Ultrafast surface vibrational dynamics," *Surf. Sci. Reports*, vol. 65, p. 45, 2010.

[17] J. Bdzoch, *Ultrafast Energy and Charge Transfer in D_2O/Ru(0001)*. PhD thesis, Freie Universität Berlin, 2010.

[18] A. J. Bard and L. R. Faulkner, *Electrochemical Methods: Fundamentals and Applications*. Wiley, 2001.

[19] M. Osawa, K. Komatsu, G. Samjeske, T. Uchida, T. Ikeshoji, A. Cuesta, and C. Gutierrez, "The Role of Bridge-Bonded Adsorbed Formate in the Electrocatalytic Oxidation of Formic Acid on Platinum," *Angew. Chem., Int. Ed.*, vol. 50, pp. 1159–1163, 2010.

Acknowledgements

First of all I want to thank Prof. Dr. Martin Wolf for giving me the great opportunity to write my Bachelor thesis in the Fritz–Haber–Institut.

I also want to thank Dr. Kramer Campen for providing me with this interesting topic for my thesis and being a group leader I could always come to if I needed something.

A special thanks goes to Dr. Yujin Tong for being my advisor, who guided me along my way. Thank you for showing me everything I needed to know and for always being open to my questions and problems, even during your holidays.

Furthermore, I want to thank Sabine Wasle, who was my person to go to concerning everything electrochemical providing me with everything I needed and most often bringing it over herself.

I also thank everyone in the workgroup Campen for always having an open ear and simply making this a very enjoyable experience.

Eidesstattliche Erklärung gemäß § 11 Abs. 3 DPO

Ich versichere hiermit an Eides statt, dass diese Arbeit von niemand anderem als meiner Person verfasst worden ist. Alle verwendeten Hilfsmittel wie Berichte, Bücher, Internetseiten oder ähnliches sind im Literaturverzeichnes angegeben. Zitate aus fremden Arbeiten sind als solche kenntlich gemacht. Die Arbeit wurde bisher in gleicher oder ähnlicher Form keiner anderen Prüfungskommission vorgelegt und auch nicht veröffentlicht.

Berlin, den 29.07.2014